frontiers | Frontiers in Neurology

TYPE Original Research
PUBLISHED 13 January 2025
DOI 10.3389/fneur.2024.1544578

OPEN ACCESS

EDITED BY
Shuai Ren,
Affiliated Hospital of Nanjing University of Chinese Medicine, China

REVIEWED BY
Xiaowei Han,
Quzhou City People's Hospital, China
Jiajia Zhu,
First Affiliated Hospital of Anhui Medical University, China
Yuto Uchida,
Johns Hopkins Medicine, United States

*CORRESPONDENCE
Fei Chen
✉ shuibin1988@163.com
Zhenyu Dai
✉ ycsydzy@163.com
Pinglei Pan
✉ panpinglei@163.com

†These authors have contributed equally to this work and share first authorship

RECEIVED 13 December 2024
ACCEPTED 30 December 2024
PUBLISHED 13 January 2025

CITATION
Wang Z, Shen Y, Zhang X, Li Q, Dong C, Wang S, Sun H, Chen M, Xu X, Pan P, Dai Z and Chen F (2025) Prognostic value of multi-PLD ASL radiomics in acute ischemic stroke.
Front. Neurol. 15:1544578.
doi: 10.3389/fneur.2024.1544578

Prognostic value of multi-PLD ASL radiomics in acute ischemic stroke

Zhenyu Wang[1†], Yuan Shen[2†], Xianxian Zhang[2†], Qingqing Li[3], Congsong Dong[4], Shu Wang[4], Haihua Sun[2], Mingzhu Chen[2], Xiaolu Xu[2], Pinglei Pan[2,5*], Zhenyu Dai[1*] and Fei Chen[4,6*]

[1]Department of Radiology, Affiliated Hospital 6 of Nantong University, Medical School of Nantong University, Nantong, Jiangsu, China, [2]Department of Neurology, Affiliated Hospital 6 of Nantong University, Yancheng Third People's Hospital, Yancheng, Jiangsu, China, [3]Department of Radiology, Suzhou Wuzhong People's Hospital, Suzhou, Jiangsu, China, [4]Department of Radiology, Affiliated Hospital 6 of Nantong University, Yancheng Third People's Hospital, Yancheng, Jiangsu, China, [5]Department of Central Laboratory, Affiliated Hospital 6 of Nantong University, Yancheng Third People's Hospital, Yancheng, Jiangsu, China, [6]Medical Imaging Institute of Jiangsu Medical College, Yancheng, Jiangsu, China

Introduction: Early prognosis prediction of acute ischemic stroke (AIS) can support clinicians in choosing personalized treatment plans. The aim of this study is to develop a machine learning (ML) model that uses multiple post-labeling delay times (multi-PLD) arterial spin labeling (ASL) radiomics features to achieve early and precise prediction of AIS prognosis.

Methods: This study enrolled 102 AIS patients admitted between December 2020 and September 2024. Clinical data, such as age and baseline National Institutes of Health Stroke Scale (NIHSS) score, were collected. Radiomics features were extracted from cerebral blood flow (CBF) images acquired through multi-PLD ASL. Features were selected using least absolute shrinkage and selection operator regression, and three models were developed: a clinical model, a CBF radiomics model, and a combined model, employing eight ML algorithms. Model performance was assessed using receiver operating characteristic curves and decision curve analysis (DCA). Shapley Additive exPlanations was applied to interpret feature contributions.

Results: The combined model of extreme gradient boosting demonstrated superior predictive performance, achieving an area under the curve (AUC) of 0.876. Statistical analysis using the DeLong test revealed its significant outperformance compared to both the clinical model (AUC = 0.658, $p < 0.001$) and the CBF radiomics model (AUC = 0.755, $p = 0.002$). The robustness of all models was confirmed through permutation testing. Furthermore, DCA underscored the clinical utility of the combined model. The prognostic prediction of AIS was notably influenced by the baseline NIHSS score, age, as well as texture and shape features of CBF.

Conclusion: The integration of clinical data and multi-PLD ASL radiomics features in a model offers a secure and dependable approach for predicting the prognosis of AIS, particularly beneficial for patients with contraindications to contrast agents. This model aids clinicians in devising individualized treatment plans, ultimately enhancing patient prognosis.

KEYWORDS

acute ischemic stroke, radiomics, arterial spin labeling, cerebral blood flow, machine learning

1 Introduction

Stroke is defined by a range of clinical syndromes featuring focal neurological impairments triggered by cerebrovascular occurrences, standing as the third leading contributor to mortality and disability worldwide (1, 2). Acute ischemic stroke (AIS) is the predominant type of stroke, accounting for approximately 87% of all cases (3). A negative prognosis confronts approximately one-third of patients with AIS, causing a marked deterioration in their quality of life and imposing a significant financial burden on society (4). The mortality and incidence rates of AIS have decreased in recent years due to advancements in medical technology. Nevertheless, the increasing global aging population could compound the existing burden (5). Therefore, it is crucial for clinicians to promptly and precisely evaluate the prognosis of AIS to tailor individualized treatment approaches.

AIS occurs when arteries become obstructed in certain regions, causing brain tissue to death due to inadequate oxygen and glucose delivery (6). The survival of brain tissue and functional recovery, as well as the prognosis of AIS, are directly influenced by cerebral blood flow (CBF) in the infarcted area (7). The evaluation of CBF is predominantly conducted through imaging modalities, such as dynamic susceptibility contrast perfusion-weighted imaging (DSC-PWI) and computed tomography perfusion (CTP) (8). However, the use of gadolinium or iodine contrast agents is limited by allergic reactions and potential renal function impairment, which restricts their widespread clinical application (9). Arterial spin labeling (ASL) is a magnetic resonance imaging (MRI) technique that quantifies CBF by applying a pulse signal to water molecules in arterial blood, serving as an endogenous contrast agent (10). Compared to traditional imaging techniques, ASL eliminates the need for exogenous contrast agents and provides several notable advantages, such as repeated usability within a short timeframe, non-radiative properties, and reduced examination costs (11). In recent years, there has been a growing utilization of ASL imaging for evaluating blood perfusion in AIS (12, 13).

Post-labeling delay (PLD) is a critical parameter in ASL technology, representing the time between the application of the labeling pulse and the acquisition of the signal (14). However, variations in arterial transit time (ATT) across brain tissues lead to a certain degree of underestimation of CBF in single-PLD ASL technology (15). To address this limitation, multi-PLD ASL technology encodes multiple PLDs within a single scan, allowing for the measurement of ATT in brain tissue and the correction of CBF for ATT (12). This effectively addresses the problem of underestimating CBF due to single-PLD scanning (16). In areas of infarction characterized by reduced blood flow, it is essential to make this correction to prevent underestimation of perfusion (17). Multi-PLD ASL has shown robust agreement with CBF measurements acquired through DSC-PWI or CTP (18–20).

Mihoko et al. employed multi-PLD ASL technology to determine the correlation between CBF and the initial severity of AIS (21). Furthermore, Li et al. discovered that the Alberta Stroke Program Early CT Score, determined through multi-PLD ASL, serves as a standalone prognostic indicator in AIS (22). Consequently, multi-PLD ASL shows promise as an alternative method for assessing the severity and prognosis of AIS. However, the quantification of CBF in the aforementioned studies offers a restricted evaluation of perfusion status and overlooks the heterogeneity present within the lesion.

Radiomics enables the rapid, objective, and high-throughput extraction of numerous features from biomedical images (23). This process reflects subtle changes that are challenging to detect visually, thereby offering a more comprehensive array of biological information (24). Guo et al. uncovered a significant correlation between the dynamic radiomics features of DSC-PWI in the infarcted region and the clinical prognosis of AIS patients at 90 days (25). However, research focusing on the ASL radiomics features of AIS patients remains limited. Therefore, we hypothesize that CBF radiomics features based on multi-PLD-ASL have significant value in the prognostic assessment of AIS patients.

In this study, our aim is to utilize machine learning (ML) techniques to construct multi-PLD ASL radiomics models for predicting the prognosis of AIS. Moreover, relevant clinical risk factors will be incorporated to improve predictive precision and determine the optimal prognostic model.

2 Materials and methods

2.1 Patients

A cohort of 102 patients with AIS (45.10% female; mean [SD] age, 67.98 [12.49] years) was recruited at the Third People's Hospital of Yancheng between December 2020 and September 2024. The screening procedures and research analysis are depicted in Figure 1.

The inclusion criteria were: (1) a confirmed diagnosis of AIS according to the guidelines (26); (2) the ability to cooperate with brain MRI scans within 24–72 h after symptom onset; (3) a modified Rankin Scale (mRS) score of 0 before symptom onset; and (4) individuals aged 18 or older.

The exclusion criteria were: (1) posterior circulation infarction; (2) intracranial occupying lesions such as tumors or arachnoid cysts; (3) significant MRI artifacts; (4) evidence of hemorrhagic transformation; and (5) patients with severe diseases in other systems.

2.2 Clinical assessment

Demographic and clinical data were gathered for all participants, including age, gender, onset to therapy time, baseline National Institutes of Health Stroke Scale (NIHSS) score, treatment strategies, atrial fibrillation, hypertension, diabetes mellitus, hyperlipidemia, coronary heart disease, smoking history, alcohol abuse and history of stroke. To aid in the modeling process, the continuous variables in the dataset were standardized to mitigate disparities in data distribution. The mRS score was assessed through a telephone follow-up at 90 days

Abbreviations: AIS, acute ischemic stroke; CBF, cerebral blood flow; DSC-PWI, dynamic sensitivity contrast perfusion weighted imaging; CTP, computed tomography perfusion; ASL, arterial spin labeling; MRI, magnetic resonance imaging; PLD, post-labeling delay; ATT, arterial transit time; ML, machine learning; mRS, modified Rankin Scale; NIHSS, National Institutes of Health Stroke Scale; DWI, diffusion weighted imaging; ROI, region of interest; ICC, interclass correlation coefficient; XGBoost, extreme gradient boosting; LOOCV, leave-one-out cross-validation; LASSO, least absolute shrinkage and selection operator; ROC, receiver operating characteristic; AUC, area under the curve; PR-AUC, precision-recall AUC; DCA, decision curve analysis; SHAP, Shapley Additive exPlanations; CI, confidence interval.

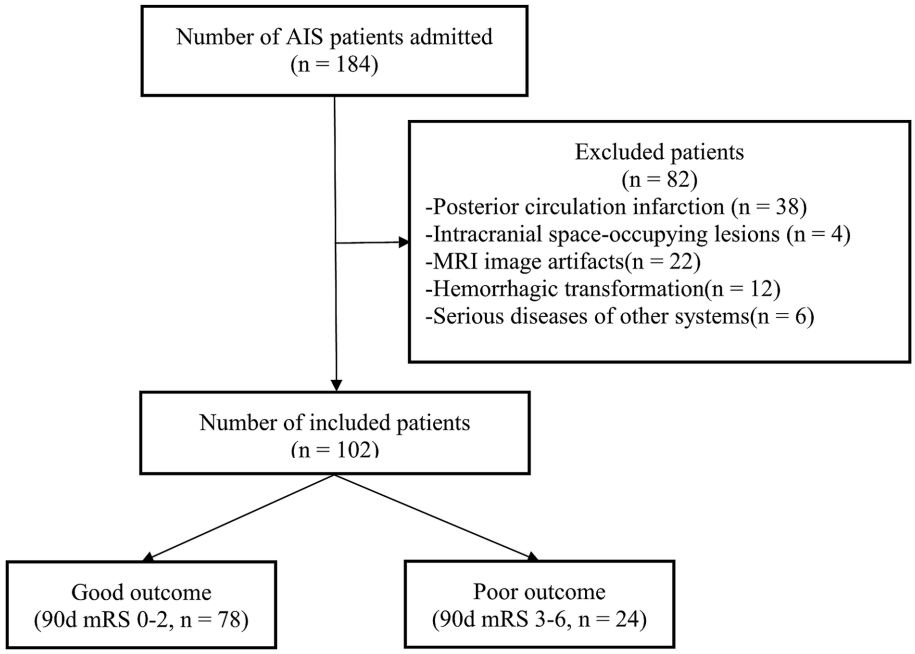

FIGURE 1
Study enrollment process. AIS, acute ischemic stroke; MRI, magnetic resonance imaging; mRS, modified Rankin Scale.

post-onset, classifying prognosis as either good (mRS score ≤ 2) or poor (mRS score > 2).

2.3 MRI acquisition

All participants underwent head MRI scans (3.0T, GE Discovery 750 W, USA), including diffusion weighted imaging (DWI) and multi-PLD ASL sequences within 24–72 h after symptom onset. Multi-PLD ASL employs a three-dimensional pseudo-continuous scanning method, with the following specific parameters: echo time: 5978 ms; repetition time: 11.5 ms; field of view: 22 × 22 cm; slice thickness: 4.5 mm; slice number: 106; resolution: 4.67 mm * 4.67 mm; NEX: 1; PLDs: 1.0 s, 1.22 s, 1.48 s, 1.78 s, 2.1 s, 2.63 s, 3.32 s; scan duration: 6 min 2 s. The ATT-corrected CBF image is obtained by averaging the individual CBF images calculated for each PLD directly on the MRI scanner.

2.4 Lesion segmentation and radiomics feature extraction

To improve the image quality, N4 bias field correction was applied to the obtained CBF images to minimize the impact of magnetic field inhomogeneity. Subsequently, the DWI images were used as a template to conduct image registration with the CBF images. Two radiologists independently delineated the infarct area slice-by-slice on DWI images using ITK-SNAP[1] to define the region of interest (ROI). The ROI was then transferred to the corresponding registered CBF images. PyRadiomics software (version: 3.1.0) was utilized to extract 1,032 features from the CBF image ROI. The intraclass correlation coefficient (ICC) was computed to evaluate the consistency of the extracted features. Features with an ICC exceeding 0.75 were deemed highly consistent, standardized, and incorporated into the model development process.

2.5 Model building and evaluation

Eight different ML methods were employed to build models, including logistic regression, support vector machine, random forest, k-nearest neighbors, naive Bayes, extreme gradient boosting (XGBoost), light gradient boosting machine and deep neural networks. Given the limited sample size included in this study, leave-one-out cross-validation (LOOCV) was employed instead of partitioning the subjects into training and testing sets. This method involves utilizing (N-1) samples for training across N iterations, while reserving one sample as the test set in each iteration. This strategy aims to enhance data utilization and increase accuracy levels (27). In each training cycle, the least absolute shrinkage and selection operator (LASSO) regression was used to select features with non-zero coefficients through 10-fold cross-validation.

Class-weighted loss functions were utilized in model training to address the effects of class imbalance. In order to reduce bias toward the majority class (good prognosis), the minority class (poor prognosis) was assigned higher weights to amplify its influence on the loss function. Grid search was utilized for hyperparameter tuning across all models. This approach systematically investigated various combinations of model-specific hyperparameters (e.g., the penalty parameter C for logistic regression, the kernel type and gamma for

1 http://www.itk-snap.org, version 4.0.

TABLE 1 Demographic and clinical characteristics of the good and poor prognosis groups.

Characteristics	Good (n = 78)	Poor (n = 24)	$t/Z/\chi^2$	p value
Age, year[a]	66 ± 12	73 ± 13	−2.283	0.025*
Female, n (%)	33 (42.31)	13 (54.17)	1.042	0.307
Onset to therapy time, hour[a]	13.42 ± 14.90	13.23 ± 13.89	0.055	0.956
Baseline NIHSS score[b]	3 (1, 6)	8 (4, 12)	4.505	<0.001*
Reperfusion therapy, n (%)	18 (23.08)	6 (25.00)	0.038	0.846
Atrial fibrillation, n (%)	12 (15.38)	5 (20.83)	0.392	0.531
Hypertension, n (%)	58 (74.36)	18 (75.00)	0.004	0.950
Diabetes mellitus, n (%)	22 (28.21)	6 (25.00)	0.095	0.758
Hyperlipidemia, n (%)	16 (20.51)	5 (20.83)	0.001	0.973
Coronary heart disease, n (%)	3 (3.85)	2 (8.33)	0.793	0.373
Smoking history, n (%)	19 (24.36)	4 (16.67)	0.622	0.430
Alcohol abuse, n (%)	13 (16.67)	3 (12.50)	0.241	0.624
History of stroke, n (%)	10 (12.82)	7 (29.17)	3.531	0.060

n, number of cases.
[a]($\bar{x} \pm s$).
[b][M (Q1, Q3)].
NIHSS, National Institutes of Health Stroke Scale. The marked with "*" is statistically significant ($p < 0.05$).

support vector machine, the number of estimators and maximum depth for random forest, XGBoost, and light gradient boosting machine) to determine the optimal configuration for each method. The optimal hyperparameters were chosen according to performance metrics obtained from cross-validation.

We constructed CBF radiomics models using radiomics features and clinical models using clinical data. Furthermore, combined models were established by integrating radiomics features and clinical data. Receiver operating characteristic (ROC) curves were generated for all models to evaluate performance based on the area under the curve (AUC), sensitivity, specificity, accuracy, and F1 score. The model's performance on the minority class (poor prognosis) was also examined through the evaluation of precision, recall, F1-score, and the area under the precision-recall AUC (PR-AUC). Additionally, the robustness of the models was validated through 5,000 permutation tests. The DeLong test was utilized to statistically compare the predictive performance of the models. Decision curve analysis (DCA) was performed to assess the potential clinical net benefits of the models. Finally, feature importance was determined within the models using SHapley Additive exPlanations (SHAP).

2.6 Statistical analysis

Statistical analysis was conducted using SPSS software (Version 26.0, IBM, Armonk, NY, USA). Clinical data were evaluated for normality and homogeneity of variance. Data following a normal distribution were expressed as mean ± standard deviation. In cases where the data showed a non-normal distribution, the descriptive measure employed was the median (first quartile, third quartile). Continuous variables were analyzed using the independent samples t-test or the Mann–Whitney U test, whereas categorical variables were analyzed with the chi-square test. Statistical significance was defined as $p < 0.05$.

A statistical power analysis was conducted to assess the adequacy of the sample size in supporting the study's conclusions. The analysis was based on the observed AUC values and a null hypothesis AUC of 0.5 (random classification).

Python (version 3.11)[2] was used for image processing and model construction. The 'sklearn' package was used to perform LASSO regression analysis for feature selection. The 'matplotlib' package was used to generate ROC and DCA curves. The 'SHAP' package was implemented to calculate SHAP values for the features.

3 Results

3.1 Demographic characteristics of patients

The demographic and clinical data of the included AIS patients are detailed in Table 1. Among all patients, 78 exhibited a good prognosis, while 24 had a poor prognosis. In comparison to patients with a good prognosis, those with a poor prognosis were older ($p = 0.025$) and displayed a higher baseline NIHSS score ($p < 0.001$). No significant differences were observed between the two groups in terms of gender, onset to therapy time, treatment strategies, atrial fibrillation, hypertension, diabetes mellitus, hyperlipidemia, coronary heart disease, smoking history, alcohol abuse, or history of stroke.

3.2 Model building and performance

Out of the eight ML methods, the model constructed with the XGBoost algorithm exhibited superior performance. The

2 https://www.python.org

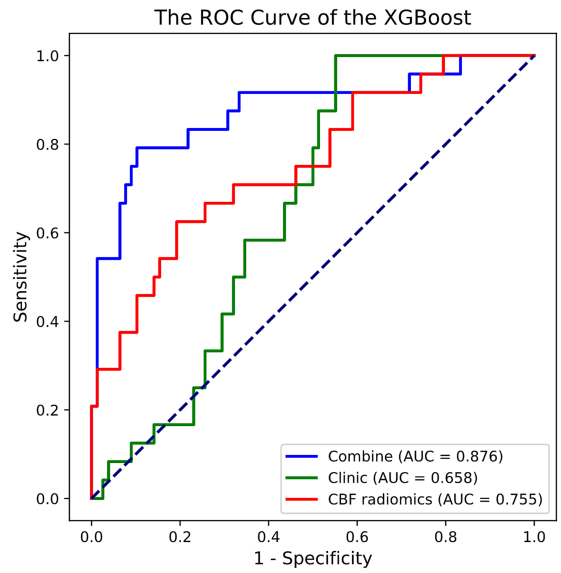

FIGURE 2
ROC curve of the XGBoost models in predicting prognosis of acute ischemic stroke. ROC, receiver operating characteristic; XGBoost, extreme gradient boosting; AUC, area under the curve; CBF, cerebral blood flow.

hyperparameters for XGBoost were configured with a maximum depth of 6, a learning rate of 0.3, 100 estimators, a subsample of 1, and column sampling by tree set to 1. Figure 2 and Table 2 display the ROC curves and key diagnostic performance metrics for each XGBoost models. The results of the models created using the remaining seven ML algorithms are elucidated in the Supplementary material.

Among the XGBoost models, the combined model demonstrated superior performance, attaining an AUC of 0.876 (95% CI, 0.768–0.960), indicating its significant capability in discriminating between good and poor prognoses. In comparison, the AUC for the clinical model was 0.658 (95% CI, 0.547–0.755), while the AUC of the CBF radiomics model was 0.755 (95% CI, 0.635–0.869). The DeLong test demonstrated that the combined model exhibited markedly better predictive performance compared to both the clinical model ($p < 0.001$) and the CBF radiomics model ($p = 0.002$). Furthermore, there was no statistically significant difference between the clinical model and the CBF radiomics model ($p = 0.222$). During the 5,000 permutation tests, it is noteworthy that all models exhibited a relatively high level of robustness. In Figure 3, the DCA for all models reveals that the combined model exhibits superior net benefit compared to both the clinical model and the CBF radiomics model across a broad spectrum of threshold probabilities, ranging from 0.1 to 0.9.

Based on the observed AUC of the combined model (AUC = 0.876) and a null hypothesis AUC of 0.5, a statistical power analysis resulted in a standard error of 0.034 and a Z-value of 10.970 ($p < 0.05$), demonstrating that the current dataset possesses adequate power (>80%) to validate the observed AUC. Furthermore, the combined model achieved a precision of 0.79, recall of 0.83, PR-AUC of 0.85, and F1-score of 0.81 for the minority group, indicating its ability to accurately identify cases with poor prognosis.

3.3 Model interpretability

As illustrated in Figure 4, we used the SHAP values from the best-performing XGBoost combined model to identify the important variables for predicting AIS prognosis. Positive SHAP values were linked to an elevated risk of poor prognosis, while negative SHAP values were indicative of a greater chance of poor prognosis. Notably, the baseline NIHSS score and age played significant roles in predicting the prognosis of AIS. Additionally, several texture and shape features derived from the CBF images also contributed significantly to the predictive performance of the model.

4 Discussion

This study proposes a novel approach that integrates multi-PLD ASL radiomics features with clinical variables for predicting AIS prognosis. Among the models developed, the XGBoost algorithm exhibited the highest AUC value of 0.876, underscoring its predictive accuracy for AIS prognosis. It can assist clinicians in early prognostic assessment and the implementation of personalized treatment plans, ultimately aiming to reduce the incidence of poor prognosis.

The fundamental aspect of AIS involves tissue necrosis caused by embolism in the supplying artery. CBF serves as a direct reflection of the hemodynamic condition within the infarcted region, making it a pivotal indicator of brain tissue injury and a key role in evaluating neurological rehabilitation (28). In contrast to conventional DSC-PWI, multi-PLD ASL technology produces CBF images without the need for contrast agents (29). Moreover, radiomics techniques enable the extraction of multidimensional features from medical images, providing a more thorough assessment of the heterogeneity of blood perfusion within lesions in comparison to visual evaluation or basic CBF quantification (30). Guo et al. developed ten ML models based on the dynamic radiomics features of DSC-PWI in the infarcted area to predict the prognosis of AIS, achieving a maximum AUC of 0.882 (25). However, there is a scarcity of studies investigating the correlation between the radiomics features of CBF in the infarcted region and the prognosis of AIS. Therefore, we aimed to develop a CBF radiomics model for AIS prognosis prediction based on multi-PLD ASL imaging. Our model attained a maximum AUC of 0.755 in the results, indicating the viability of utilizing multi-PLD ASL technology for predicting neurological recovery in AIS patients. After including age and baseline NIHSS score, the model achieves an AUC of 0.876, which aligns closely with the findings of Guo et al.'s model (25). Therefore, this method presents a safer and more reproducible avenue for prognostic prediction in AIS patients, particularly for those with contraindications to contrast agents. Moreover, the absence of contrast agents renders ASL a more economical method.

When examining the demographic and clinical profiles of AIS patients, it was observed that those with poorer prognoses were characterized by advanced age and a higher baseline NIHSS score. The development of a predictive model utilizing demographic and clinical factors yielded limited performance, as indicated by an AUC of 0.658, which falls below that of the CBF radiomics model. While the DeLong test did not indicate a statistically significant distinction between the two models, the test's power may have been constrained by the small sample size (31). Consequently, there is justification to argue for the

TABLE 2 The performance of XGBoost models in predicting prognosis of AIS patients.

Models	AUC (95% CI)	Sensitivity	Specificity	Accuracy	F1 score	Permutation test
Clinic	0.658 (0.547–0.755)	1	0.449	0.578	0.527	0.012*
CBF radiomics	0.755 (0.635–0.869)	0.625	0.808	0.765	0.556	0.002*
Combined	0.876 (0.768–0.960)	0.792	0.897	0.873	0.745	<0.001*

XGBoost, extreme gradient boosting; AIS, acute ischemic stroke; CBF, cerebral blood flow; AUC, area under the curve; CI, confidence interval. The marked with "*" is statistically significant ($p < 0.05$).

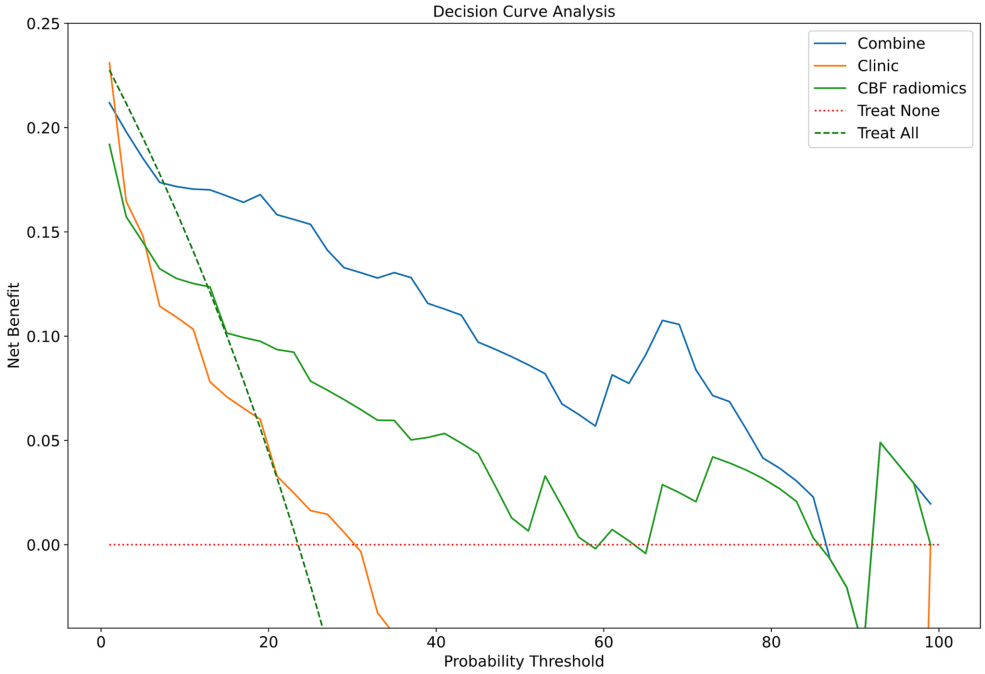

FIGURE 3
Clinical decision curve analysis of the XGBoost models. XGBoost, extreme gradient boosting; CBF, cerebral blood flow.

superiority of the CBF radiomics model compared to the clinical model. During the acute phase of AIS, the CBF radiomics model may function as an alternative to the clinical model for prognostic prediction, especially beneficial for patients with insufficient clinical data.

The combined model, which integrates clinical data with CBF radiomics features, achieved an AUC of 0.876. The DeLong test demonstrated that the combined model significantly outperformed both the clinical model and the CBF radiomics model. This finding implies that clinical data provide only partial insight into prognosis. In contrast, CBF radiomics features provide distinct information on alterations in cerebral blood perfusion status that clinical data alone cannot encompass. This discovery is in line with results from various studies, underscoring the essential role of the complementarity of multimodal information in radiomics research (32). Additionally, the DCA demonstrated that the combined model yielded a higher net benefit across a wide range of threshold probabilities. This suggests that the model has the potential for application in clinical practice, with the only requirement being the extraction of relevant clinical and imaging data from electronic medical records and imaging systems. It can assist clinicians in delivering consistent prognostic evaluations in diverse clinical scenarios, enhancing the management of AIS by facilitating prompt interventions and optimizing resource distribution.

In order to determine the factors influencing the prognosis of AIS, we conducted SHAP analysis to assess the individual contribution of each feature to the predictive accuracy of the combined model. The baseline NIHSS score and age emerged as the most significant predictors among the clinical variables, aligning with prior studies (33–35). The baseline NIHSS score reflects stroke severity, correlating strongly with infarct size and functional outcomes in AIS patients (36). Advanced age, characterized by diminished neural plasticity and a higher prevalence of comorbidities, is a firmly established risk factor for poor outcomes in AIS (37, 38). Texture features and shape features derived from multi-PLD ASL CBF were identified as important contributors to the model. Among the texture features, the gray level run length matrix made the greatest contribution, quantifying gray intensity patterns and their spatial relationships within the ischemic area (39). Ischemic regions often exhibit varying degrees of blood flow reduction and tissue damage, and texture features can capture these variations, distinguishing areas of hypoperfusion, penumbra, and infarct core. Moreover, alterations in tissue density induced by cytotoxic and vasogenic edema may manifest in texture

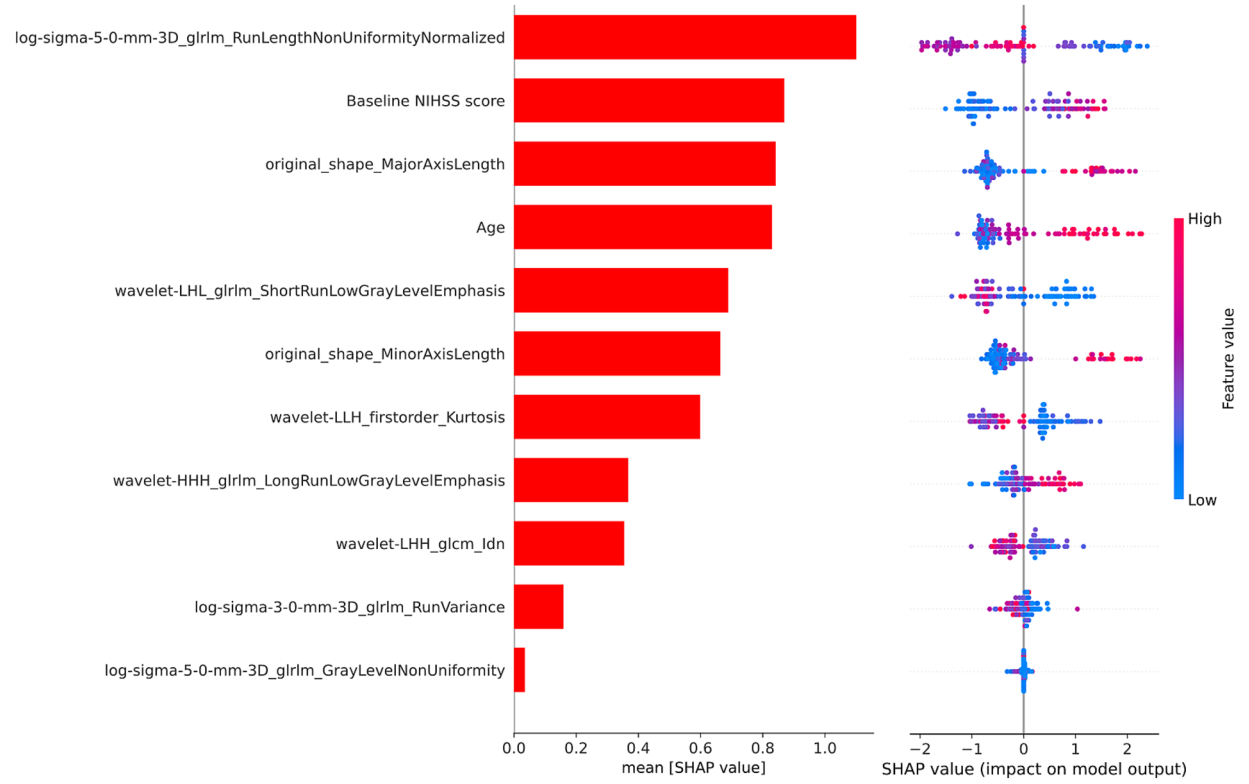

FIGURE 4
The SHAP values of the XGBoost combined model. SHAP, SHapley Additive Explanations; XGBoost, extreme gradient boosting; NIHSS, National Institutes of Health Stroke Scale.

characteristics, elucidating the advancement of secondary damage (40). Additionally, microstructural disruptions, such as the loss of neural integrity or capillary breakdown, may manifest as increased texture irregularities in radiomics analysis (41). Shape features provide evidence linking lesion geometry to the underlying vascular anatomy and collateral perfusion (42). Larger or irregularly shaped lesions may indicate more extensive vascular occlusion or failure of collateral circulation, both of which are associated with poor prognosis (43, 44). Moreover, regions with poor perfusion are more prone to displaying irregular lesion morphologies (45). These findings highlight the capability of CBF radiomics features to reflect the extent and heterogeneity of tissue damage, demonstrating their relevance to clinical prognosis of AIS.

This study must acknowledge several limitations. Firstly, the small sample size may restrict the generalizability of the results. Despite utilizing LOOCV and permutation tests to mitigate this issue, larger multi-center datasets are essential to confirm the model and broaden its external applicability. Secondly, the exclusion of posterior circulation infarction cases restricted the model's generalizability. Future research should incorporate posterior circulation cases into larger datasets to construct subtype-specific models. Thirdly, despite efforts to ensure consistency through ICC analysis, manual delineation of infarcted areas may lead to observer variability (46). Future research should explore automated or semi-automated segmentation methods to reduce subjectivity and improve reproducibility. Fourthly, this study focused exclusively on the multi-PLD ASL sequence. Future studies should explore integrating multimodal imaging techniques, such as quantitative susceptibility mapping and diffusion-prepared ASL, to better understand AIS progression by delineating the ischemic penumbra and assessing blood–brain barrier integrity (47–50). Finally, future studies could integrate radiomics features with network-based approaches, which have proven valuable in neuropsychiatric disorders, to better understand how ischemic lesions disrupt brain networks and influence prognosis of AIS (51–53).

5 Conclusion

In this study, we established new prognostic prediction models for AIS utilizing multi-PLD ASL technology. The results indicate that the combined model, which integrates clinical data and CBF radiomics features, accurately predicts AIS prognosis. This model has the potential to assist clinicians in identifying individualized treatment approaches to improve patient prognosis. This strategy presents a feasible alternative for assessing the prognosis of AIS, especially in individuals for whom the use of contrast agents is contraindicated.

Data availability statement

The original contributions presented in the study are included in the article/Supplementary material, further inquiries can be directed to the corresponding authors.

Ethics statement

The studies involving humans were approved by the Ethics Committee of the Yancheng Third People's Hospital. The studies were conducted in accordance with the local legislation and institutional requirements. The participants provided their written informed consent to participate in this study. Written informed consent was obtained from the individual(s) for the publication of any potentially identifiable images or data included in this article.

Author contributions

ZW: Methodology, Writing – original draft. YS: Supervision, Writing – review & editing. XZ: Formal analysis, Methodology, Writing – review & editing. QL: Conceptualization, Data curation, Writing – review & editing. CD: Data curation, Methodology, Writing – review & editing. SW: Conceptualization, Data curation, Writing – review & editing. HS: Conceptualization, Methodology, Supervision, Writing – review & editing. MC: Methodology, Supervision, Writing – review & editing. XX: Data curation, Methodology, Writing – review & editing. PP: Conceptualization, Methodology, Writing – review & editing. ZD: Project administration, Supervision, Writing – review & editing. FC: Data curation, Supervision, Writing – review & editing.

Funding

The author(s) declare financial support was received for the research, authorship, and/or publication of this article. This work was supported by the Elderly Health Research Project of Jiangsu Province (No. LKM2024050), the Research Foundation of Science and Technology Bureau of Yancheng (No. YCBK2023041), the Medical and Scientific Development Program of Yancheng of Jiangsu Province of China (No. YK2020070, YK2023088), the Special Project of Clinical Medicine of Nantong University (No. YXY-Z2023003, 2024LZ004), the Special Funds for Science Development of the Yancheng Third People's Hospital of Jiangsu Vocational College of Medicine (No. 20229103), and the School-Local Collaborative Innovation Research Project of Jiangsu Vocational College of Medicine (No. 20239102).

Acknowledgments

We would like to thank all the individuals who took part in the study.

Conflict of interest

The authors declare that the research was conducted in the absence of any commercial or financial relationships that could be construed as a potential conflict of interest.

Generative AI statement

The author(s) declare that no Gen AI was used in the creation of this manuscript.

Publisher's note

Supplementary material

The Supplementary material for this article can be found online at: https://www.frontiersin.org/articles/10.3389/fneur.2024.1544578/full#supplementary-material

References

1. Feigin VL, Brainin M, Norrving B, Martins S, Sacco RL, Hacke W, et al. World stroke organization (WSO): global stroke fact sheet 2022. *Int J Stroke*. (2022) 17:18–29. doi: 10.1177/17474930211065917

2. Feigin VL, Stark BA, Johnson CO, Roth GA, Bisignano C, Abady GG, et al. Global, regional, and national burden of stroke and its risk factors, 1990–2019: a systematic analysis for the global burden of disease study 2019. *Lancet Neurol*. (2021) 20:795–820. doi: 10.1016/S1474-4422(21)00252-0

3. Saini V, Guada L, Yavagal DR. Global epidemiology of stroke and access to acute ischemic stroke interventions. *Neurology*. (2021) 97:S6–S16. doi: 10.1212/WNL.0000000000012781

4. Wu S, Wu B, Liu M, Chen Z, Wang W, Anderson CS, et al. Stroke in China: advances and challenges in epidemiology, prevention, and management. *Lancet Neurol*. (2019) 18:394–405. doi: 10.1016/S1474-4422(18)30500-3

5. Béjot Y, Bailly H, Graber M, Garnier L, Laville A, Dubourget L, et al. Impact of the ageing population on the burden of stroke: the Dijon stroke registry. *Neuroepidemiology*. (2019) 52:78–85. doi: 10.1159/000492820

6. Hofmeister J, Bernava G, Rosi A, Vargas MI, Carrera E, Montet X, et al. Clot-based Radiomics predict a mechanical Thrombectomy strategy for successful recanalization in acute ischemic stroke. *Stroke*. (2020) 51:2488–94. doi: 10.1161/STROKEAHA.120.030334

7. Nakamura K, Ago T. Pericyte-mediated molecular mechanisms underlying tissue repair and functional recovery after ischemic stroke. *J Atheroscler Thromb*. (2023) 30:1085–94. doi: 10.5551/jat.RV22007

8. Dani KA, Thomas RGR, Chappell FM, Shuler K, MacLeod MJ, Muir KW, et al. Computed tomography and magnetic resonance perfusion imaging in ischemic stroke: definitions and thresholds. *Ann Neurol*. (2011) 70:384–401. doi: 10.1002/ana.22500

9. Bivard A, Stanwell P, Levi C, Parsons M. Arterial spin labeling identifies tissue salvage and good clinical recovery after acute ischemic stroke. *J Neuroimaging*. (2013) 23:391–6. doi: 10.1111/j.1552-6569.2012.00728.x

10. Haller S, Zaharchuk G, Thomas DL, Lovblad KO, Barkhof F, Golay X. Arterial spin labeling perfusion of the brain: emerging clinical applications. *Radiology*. (2016) 281:337–56. doi: 10.1148/radiol.2016150789

11. Hernandez-Garcia L, Lahiri A, Schollenberger J. Recent progress in ASL. *Neuroimage*. (2019) 187:3–16. doi: 10.1016/j.neuroimage.2017.12.095

12. Lindner T, Bolar DS, Achten E, Barkhof F, Bastos-Leite AJ, Detre JA, et al. Current state and guidance on arterial spin labeling perfusion MRI in clinical neuroimaging. *Magn Reson Med*. (2023) 89:2024–47. doi: 10.1002/mrm.29572

13. Sui B, Gao P. Imaging evaluation of acute ischemic stroke. *J Int Med Res*. (2020) 48:1–5. doi: 10.1177/0300060518802530

14. Golay X, Ho M-L. Multidelay ASL of the pediatric brain. *Br J Radiol*. (2022) 95:20220034. doi: 10.1259/bjr.20220034

15. Mutsaerts HJMM, Petr J, Václavů L, van Dalen JW, Robertson AD, Caan MW, et al. The spatial coefficient of variation in arterial spin labeling cerebral blood flow images. *J Cereb Blood Flow Metab*. (2017) 37:3184–92. doi: 10.1177/0271678X16683690

16. Woods JG, Achten E, Asllani I, Bolar DS, Dai W, Detre JA, et al. Recommendations for quantitative cerebral perfusion MRI using multi-timepoint arterial spin labeling: acquisition, quantification, and clinical applications. *Magn Reson Med*. (2024) 92:469–95. doi: 10.1002/mrm.30091

17. Arrarte Terreros N, van Willigen BG, Niekolaas WS, Tolhuisen ML, Brouwer J, Coutinho JM, et al. Occult blood flow patterns distal to an occluded artery in acute ischemic stroke. *J Cereb Blood Flow Metab*. (2021) 42:292–302. doi: 10.1177/0271678X211044941

18. Yan C, Yu F, Zhang Y, Zhang M, Li J, Wang Z, et al. Multidelay arterial spin labeling versus computed tomography perfusion in penumbra volume of acute ischemic stroke. *Stroke*. (2023) 54:1037–45. doi: 10.1161/STROKEAHA.122.040759

19. Xu X, Tan Z, Fan M, Ma M, Fang W, Liang J, et al. Comparative study of multi-delay Pseudo-continuous arterial spin labeling perfusion MRI and CT perfusion in ischemic stroke disease. *Front Neuroinform*. (2021) 15:719719. doi: 10.3389/fninf.2021.719719

20. Wang DJJ, Alger JR, Qiao JX, Gunther M, Pope WB, Saver JL, et al. Multi-delay multi-parametric arterial spin-labeled perfusion MRI in acute ischemic stroke — comparison with dynamic susceptibility contrast enhanced perfusion imaging. *Neuroimage Clin*. (2013) 3:1–7. doi: 10.1016/j.nicl.2013.06.017

21. Sasahara M, Yamanaka M, Matsushita T, Abe T, Otomo M, Yamamoto Y, et al. Evaluation of the ischemic penumbra and prognosis in acute cerebral infarction using cerebral blood flow and delay time derived from multi-delay pCASL imaging. *J Med Investig*. (2024) 71:286–92. doi: 10.2152/jmi.71.286

22. Li Q, Jiang C, Qian L, Yang J, Mu T, Dong C, et al. Prognostic value of multi-PLD ASL-based cerebral perfusion ASPECTS in acute ischemic stroke. *Front Neurol*. (2024) 15:15. doi: 10.3389/fneur.2024.1476937

23. Mayerhoefer ME, Materka A, Langs G, Häggström I, Szczypiński P, Gibbs P, et al. Introduction to Radiomics. *J Nucl Med*. (2020) 61:488–95. doi: 10.2967/jnumed.118.222893

24. Guiot J, Vaidyanathan A, Deprez L, Zerka F, Danthine D, Frix AN, et al. A review in radiomics: making personalized medicine a reality via routine imaging. *Med Res Rev*. (2022) 42:426–40. doi: 10.1002/med.21846

25. Guo Y, Yang Y, Wang M, Luo Y, Guo J, Cao F, et al. The combination of whole-brain features and local-lesion features in DSC-PWI may improve ischemic stroke outcome prediction. *Life*. (2022) 12:1847. doi: 10.3390/life12111847

26. Mendelson SJ, Prabhakaran S. Diagnosis and Management of Transient Ischemic Attack and Acute Ischemic Stroke. *JAMA*. (2021) 325:1088. doi: 10.1001/jama.2020.26867

27. Cheng J, Dekkers JCM, Fernando RL. Cross-validation of best linear unbiased predictions of breeding values using an efficient leave-one-out strategy. *J Anim Breed Genet*. (2021) 138:519–27. doi: 10.1111/jbg.12545

28. Aracki-Trenkic A, Law-Ye B, Radovanovic Z, Stojanov D, Dormont D, Pyatigorskaya N. ASL perfusion in acute ischemic stroke: the value of CBF in outcome prediction. *Clin Neurol Neurosurg*. (2020) 194:105908. doi: 10.1016/j.clineuro.2020.105908

29. Hernandez-Garcia L, Aramendía-Vidaurreta V, Bolar DS, Dai W, Fernández-Seara MA, Guo J, et al. Recent technical developments in ASL: a review of the state of the art. *Magn Reson Med*. (2022) 88:2021–42. doi: 10.1002/mrm.29381

30. Yang J, Cai H, Liu N, Huang J, Pan Y, Zhang B, et al. Application of radiomics in ischemic stroke. *J Int Med Res*. (2024) 52:3000605241238141. doi: 10.1177/03000605241238141

31. Demler OV, Pencina MJ, D'Agostino RB. Misuse of DeLong test to compare AUCs for nested models. *Stat Med*. (2012) 31:2577–87. doi: 10.1002/sim.5328

32. Dragoş HM, Stan A, Pintican R, Feier D, Lebovici A, Panaitescu PS, et al. MRI radiomics and predictive models in assessing ischemic stroke outcome-a systematic review. *Diagnostics*. (2023) 13:857. doi: 10.3390/diagnostics13050857

33. Chung C-C, Su EC-Y, Chen J-H, Chen Y-T, Kuo C-Y. XGBoost-based simple three-item model accurately predicts outcomes of acute ischemic stroke. *Diagnostics*. (2023) 13:842. doi: 10.3390/diagnostics13050842

34. Ding G-y, Xu J-h, He J-h, Nie Z-y. Clinical scoring model based on age, NIHSS, and stroke-history predicts outcome 3 months after acute ischemic stroke. *Front Neurol*. (2022) 13:13. doi: 10.3389/fneur.2022.935150

35. Shrestha S, Poudel RS, Khatiwada D, Thapa L. Stroke subtype, age, and baseline NIHSS score predict ischemic stroke outcomes at 3 months: a preliminary study from Central Nepal. *J Multidiscip Healthc*. (2015) 8:443–8. doi: 10.2147/JMDH.S90554

36. Kwah LK, Diong J. National Institutes of Health Stroke Scale (NIHSS). *J Physiother*. (2014) 60:61. doi: 10.1016/j.jphys.2013.12.012

37. Ahmed R, Mhina C, Philip K, Patel SD, Aneni E, Osondu C, et al. Age- and sex-specific trends in medical complications after acute ischemic stroke in the United States. *Neurology*. (2023) 100:e1282–95. doi: 10.1212/WNL.0000000000206749

38. Gutchess A. Plasticity of the aging brain: new directions in cognitive neuroscience. *Science*. (2014) 346:579–82. doi: 10.1126/science.1254604

39. Lee J, Yoo SK, Kim K, Lee BM, Park VY, Kim JS, et al. Machine learning-based radiomics models for prediction of locoregional recurrence in patients with breast cancer. *Oncol Lett*. (2023) 26:422. doi: 10.3892/ol.2023.14008

40. Bai J, He M, Gao E, Yang G, Yang H, Dong J, et al. Radiomic texture analysis based on neurite orientation dispersion and density imaging to differentiate glioblastoma from solitary brain metastasis. *BMC Cancer*. (2023) 23:1231. doi: 10.1186/s12885-023-11718-0

41. Brown CE, Li P, Boyd JD, Delaney KR, Murphy TH. Extensive turnover of dendritic spines and vascular remodeling in cortical tissues recovering from stroke. *J Neurosci*. (2007) 27:4101–9. doi: 10.1523/JNEUROSCI.4295-06.2007

42. Pensato U, Demchuk AM, Menon BK, Nguyen TN, Broocks G, Campbell BCV, et al. Cerebral infarct growth: pathophysiology, pragmatic assessment, and clinical implications. *Stroke*. (2024) 56:219–29. doi: 10.1161/STROKEAHA.124.049013

43. Liu S, Fan D, Zang F, Gu N, Yin Y, Ge X, et al. Collateral circulation detected by arterial spin labeling predicts outcome in acute ischemic stroke. *Acta Neurol Scand*. (2022) 146:635–42. doi: 10.1111/ane.13694

44. Meng X, Ji J. Infarct volume and outcome of cerebral ischaemia, a systematic review and meta-analysis. *Int J Clin Pract*. (2021) 75:e14773. doi: 10.1111/ijcp.14773

45. Abels B, Klotz E, Tomandl BF, Kloska SP, Lell MM. Perfusion CT in acute ischemic stroke: a qualitative and quantitative comparison of deconvolution and maximum slope approach. *AJNR Am J Neuroradiol*. (2010) 31:1690–8. doi: 10.3174/ajnr.A2151

46. Sherer MV, Lin D, Elguindi S, Duke S, Tan L-T, Cacicedo J, et al. Metrics to evaluate the performance of auto-segmentation for radiation treatment planning: a critical review. *Radiother Oncol*. (2021) 160:185–91. doi: 10.1016/j.radonc.2021.05.003

47. Uchida Y, Kan H, Kano Y, Onda K, Sakurai K, Takada K, et al. Longitudinal changes in iron and myelination within ischemic lesions associate with neurological outcomes: a pilot study. *Stroke*. (2024) 55:1041–50. doi: 10.1161/STROKEAHA.123.044606

48. Uchida Y, Kan H, Inoue H, Oomura M, Shibata H, Kano Y, et al. Penumbra detection with oxygen extraction fraction using magnetic susceptibility in patients with acute ischemic stroke. *Front Neurol*. (2022) 13:752450. doi: 10.3389/fneur.2022.752450

49. Uchida Y, Kan H, Furukawa G, Onda K, Sakurai K, Takada K, et al. Relationship between brain iron dynamics and blood-brain barrier function during childhood: a quantitative magnetic resonance imaging study. *Fluids Barriers CNS*. (2023) 20:60. doi: 10.1186/s12987-023-00464-x

50. Uchida Y, Kan H, Sakurai K, Horimoto Y, Hayashi E, Iida A, et al. APOE ε4dose associates with increased brain iron and β-amyloid via blood–brain barrier dysfunction. *J Neurol Neurosurg Psychiatry*. (2022) 93:772–8. doi: 10.1136/jnnp-2021-328519

51. Mo F, Zhao H, Li Y, Cai H, Song Y, Wang R, et al. Network localization of state and trait of auditory verbal hallucinations in schizophrenia. *Schizophr Bull*. (2024) 50:1326–36. doi: 10.1093/schbul/sbae020

52. Zhang X, Xu R, Ma H, Qian Y, Zhu J. Brain structural and functional damage network localization of suicide. *Biol Psychiatry*. (2024) 95:1091–9. doi: 10.1016/j.biopsych.2024.01.003

53. Cheng Y, Cai H, Liu S, Yang Y, Pan S, Zhang Y, et al. Brain network localization of gray matter atrophy and neurocognitive and social cognitive dysfunction in schizophrenia. *Biol Psychiatry*. (2025) 97:148–56. doi: 10.1016/j.biopsych.2024.07.021